# Microstructural properties of the vertical occipital fasciculus explain the variability in human stereoacuity

Hiroki Oishi[a,b,1], Hiromasa Takemura[a,b,1,2], Shuntaro C. Aoki[b], Ichiro Fujita[a,b], and Kaoru Amano[a,b]

[a]Center for Information and Neural Networks (CiNet), National Institute of Information and Communications Technology and Osaka University, Suita 565-0871, Japan; and [b]Graduate School of Frontier Biosciences, Osaka University, Suita 565-0871, Japan

Edited by Wilson S. Geisler, University of Texas at Austin, Austin, TX, and approved October 17, 2018 (received for review March 26, 2018)

**Stereopsis is a fundamental visual function that has been studied extensively. However, it is not clear why depth discrimination (stereoacuity) varies more significantly among people than other modalities. Previous studies have reported the involvement of both dorsal and ventral visual areas in stereopsis, implying that not only neural computations in cortical areas but also the anatomical properties of white matter tracts connecting those areas can impact stereopsis. Here, we studied how human stereoacuity relates to white matter properties by combining psychophysics, diffusion MRI (dMRI), and quantitative MRI (qMRI). We performed a psychophysical experiment to measure stereoacuity and, in the same participants, we analyzed the microstructural properties of visual white matter tracts on the basis of two independent measurements, dMRI (fractional anisotropy, FA) and qMRI (macromolecular tissue volume; MTV). Microstructural properties along the right vertical occipital fasciculus (VOF), a major tract connecting dorsal and ventral visual areas, were highly correlated with measures of stereoacuity. This result was consistent for both FA and MTV, suggesting that the behavioral–structural relationship reflects differences in neural tissue density, rather than differences in the morphological configuration of fibers. fMRI confirmed that binocular disparity stimuli activated the dorsal and ventral visual regions near VOF endpoints. No other occipital tracts explained the variance in stereoacuity. In addition, the VOF properties were not associated with differences in performance on a different psychophysical task (contrast detection). These series of experiments suggest that stereoscopic depth discrimination performance is, at least in part, constrained by dorso-ventral communication through the VOF.**

diffusion MRI | vertical occipital fasciculus | stereoacuity | white matter

Stereopsis is a fundamental human visual function that has been studied over two centuries (1–7). Traditional visual neuroscience has focused on the properties of neural response toward important cues for the stereopsis, such as binocular disparity, to understand the neural computation achieving the perception of the 3D world (8–10). A series of studies have revealed a number of cortical areas involved in binocular disparity processing (9–15) and demonstrated that dorsal and ventral visual areas have complementary roles in processing different aspects of stereoscopic information (16–19).

However, there is one key question that remains unanswered: Why does the ability to discriminate depth (stereoacuity) vary among people. In fact, a number of psychophysical studies have reported a broad and often bimodal distribution of human stereoacuity, which is much less evident in other visual modalities (20–23). The neurobiological origin of such large differences in perceptual performance is unknown.

Given that several visual areas in both dorsal and ventral streams are known to be involved in stereo perception and each stream has complementary aspects for stereopsis, the anatomical properties of the white matter tracts connecting those areas should also be crucial. Vertical occipital fasciculus (VOF) (24–26), which connects dorsal and ventral visual cortices, can be one of the candidates for the tracts responsible for this interstream communication. Here, we have combined modern structural neuroimaging techniques (diffusion and quantitative MRI; dMRI and qMRI) with psychophysical measurements to assess human stereoacuity and tried to clarify how the tissue properties of visual white matter tracts may relate to the stereoacuity. In addition, we have evaluated the relationship between the endpoints of the tracts and areas activated by the same stereo stimuli using fMRI. Furthermore, we tested how these tissue properties relate to the contrast detection threshold to test whether the observed relationship between structural and psychophysical measurements are specific to stereoacuity.

## Results

**Psychophysical Experiment on Stereoacuity.** We measured the stereoacuity of 19 healthy human participants using a psychophysical experiment in which they judged a perceived depth on the basis of binocular disparity (Fig. 1*A*). Participants viewed a random dot stereogram (RDS) (2) that consisted of a central disk and surrounding ring (*SI Appendix*, Fig. S1*A*) shown at one of four positions (Up-Right, Up-Left, Down-Right, Down-Left; the center was 3° away from the fixation point). The surrounding ring was always presented at zero disparity, whereas the central disk was presented at a range of disparities across trials. Participants judged the depth of the central disk ("near" or "far") with respect to the surrounding ring. Stereoacuity was estimated by fitting a psychometric function to each participant's responses (27). Fig. 1*B* shows examples of the psychometric functions and

### Significance

**Seeing in the three-dimensional world—stereopsis—is an innate human ability, but it varies substantially among individuals. The neurobiological basis of this variability is not understood. We combined diffusion and quantitative MRI imaging with a psychophysical measurements, and found that variability in stereoacuity is associated with microstructural differences in the right vertical occipital fasciculus, a white matter tract connecting dorsal and ventral visual cortex. This result suggests that the microstructure of the pathways that support information transmission across dorsal and ventral visual areas plays an important role human stereopsis.**

Author contributions: H.O., H.T., I.F., and K.A. designed research; H.O. and H.T. performed research; H.T. and S.C.A. contributed new reagents/analytic tools; H.O. and H.T. analyzed data; and H.O., H.T., I.F., and K.A. wrote the paper.

The authors declare no conflict of interest.

This article is a PNAS Direct Submission.



Data deposition: The data for reproducing analyses and codes for replicating psychophysical experiments have been deposited on Open Science Framework (available at https://osf.io/qd8cj/).

[1]H.O. and H.T. contributed equally to this work.

[2]To whom correspondence should be addressed. Email: htakemur@nict.go.jp.

This article contains supporting information online at www.pnas.org/lookup/suppl/doi:10.1073/pnas.1804741115/-/DCSupplemental.

Published online November 14, 2018.

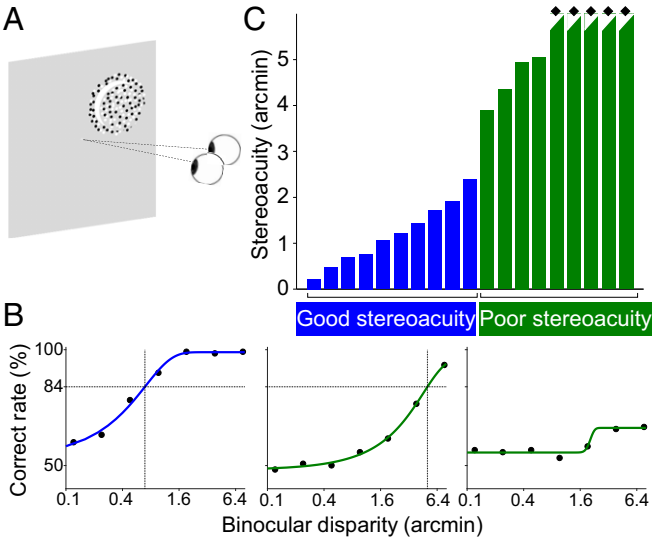


**Fig. 1.** Psychophysical experiment measuring stereoacuity. (*A*) Schematic illustration of the depth discrimination task using RDSs (see *SI Appendix*, Fig. S1*A* for details). Each RDS was concentric bipartite. Participants were asked to judge whether the central disk was nearer or farther than the surrounding disk. (*B*) The psychometric functions of three representative participants with different performances. The horizontal axis depicts binocular disparity (arcmin; logarithmic scale), while the vertical axis depicts the correct rate. The performance on the crossed and uncrossed disparities was averaged. Stereoacuity was estimated as the binocular disparity at which a participant achieved 84% correct rate (*Left* and *Middle*). *Right* shows a participant with a performance of <84% over the tested range of disparities; therefore, we could not quantitatively estimate stereoacuity using the identical criteria. (*C*) The stereoacuity of all participants ($n = 19$). The vertical axis shows the disparity threshold at which performance reached 84% correct. The stereoacuity value is arbitrary for the five participants whose stereoacuity could not be quantitatively estimated (performance < 84%; labeled with diamonds). Note, these five participants were not stereoblind (*SI Appendix, SI Materials and Methods*). We classified participants into good (blue) and poor stereoacuity (green) groups.

estimated depth discrimination threshold that corresponded to an 84% correct response rate. We succeeded in estimating the stereoacuity of 14 participants; five participants had <84% correct responses over the full range of tested disparities (±7.68 arcmin), and we were unable to determine stereoacuity from their psychometric functions. However, all participants discriminated depth from RDSs with a longer duration (500 ms) and larger disparities (15.36 arcmin) significantly better than chance, indicating that none were stereoblind (*SI Appendix, SI Materials and Methods*). We pooled trials across all stimulus locations to estimate stereoacuity because there was no notable difference in stereoacuity between left and right visual fields (*SI Appendix*, Fig. S2*A*). We confirmed that stereoacuity varied by more than one order of magnitude across participants (Fig. 1*C*), consistent with previous psychophysical studies (4, 22, 23).

**Microstructural Properties of VOF Explain Individual Variabilities in Stereoacuity.** We collected two independent structural MRI datasets, dMRI and qMRI, from the participants who took part in the psychophysical experiment. We performed tractography on the dMRI dataset to identify the trajectory of major visual white matter tracts (left and right inferior longitudinal fasciculus, ILF; left and right optic radiation, OR; forceps major of the corpus callosum; and left and right VOF) following the anatomical prescriptions in previous studies (*SI Appendix, SI Materials and Methods*). We evaluated the tissue properties along these visual white matter tracts using the widely used dMRI measure, fractional anisotropy (FA) (28), and recently proposed qMRI measure, macromolecular tissue volume (MTV), which quantifies the nonproton neural tissue density (29). Finally, we examined how the variation of FA or MTV in these visual white matter tracts correlates with the stereoacuity for each participant (see *SI Appendix*, Fig. S3 for whole-brain comparison between FA and MTV).

First, we examined white matter tracts that explained the variability in stereoacuity by comparing the performance of multiple linear regression models that predict stereoacuity from the tissue properties (MTV or FA) of the examined tracts. This analysis was performed on data from the 14 participants whose stereoacuity was quantitatively estimated (an analysis using the data of all 19 participants is also presented below). Next, we selected the best linear regression model using the Bayesian information criterion (BIC). BIC model selection for the MTV of visual white matter tracts revealed the best regression model using a single tract, the right VOF (Fig. 2*A*). This was the significant model for predicting the stereoacuity [$R^2 = 0.36$, $F_{(1,12)} = 6.71$, $P = 0.024$; Fig. 2*B* and *SI Appendix*, Table S1]. In addition, the MTV of the left ILF was a significant predictor of stereoacuity [$R^2 = 0.30$, $F_{(1,12)} = 5.22$, $P = 0.041$; *SI Appendix*, Table S1]. No other models using single, or combinations of, visual tracts were significantly correlated with the stereoacuity (*SI Appendix*, Table S1). In summary, the microstructural properties of the right VOF best predicted the variability in stereoacuity.

The BIC model selection using FA, a conventional measure of dMRI, provided similar results: The best model to explain variations in human stereoacuity included a single tract, the right VOF [$R^2 = 0.30$, $F_{(1,12)} = 5.22$, $P = 0.041$; *SI Appendix*, Fig. S4*A* and Table S1; see *SI Appendix*, Fig. S5 *A* and *B* for results in axial and radial diffusivity]. No other models, including the model using the FA of the left ILF [$R^2 = 0.12$, $F_{(1,12)} = 1.57$, $P = 0.23$], significantly predicted stereoacuity (*SI Appendix*, Table S1). These results, across two independent measurements using different pulse sequences, suggested that the observed correlation was related to neural tissue volume along the right VOF, rather than the morphological factors specifically affecting FA (e.g., crossing fibers).

We further examined how MTV and FA differed between the good stereoacuity (low disparity-threshold) and poor stereoacuity (high disparity-threshold) groups, by incorporating datasets from all participants ($n = 19$), including the five participants whose stereoacuity could not be estimated from the psychometric function analysis (Fig. 1*B*). First, we classified the participants with quantitative estimates of stereoacuity ($n = 14$) into different subgroups by applying a two-step clustering algorithm to the stereoacuity data and selecting the best clustering based on BIC (*SI Appendix, SI Materials and Methods*). The analysis revealed two subgroups, which correspond to good ($n = 10$) or poor ($n = 4$) stereoacuity groups. Then the five participants without quantitative estimates of stereoacuity were included in the poor stereoacuity group ($n = 9$ in total, Fig. 1*C*). We found that the good stereoacuity group had a significantly higher MTV (Fig. 2*C*; $d' = 1.27$, $t_{17} = 2.77$, $P = 0.013$) and FA (*SI Appendix*, Fig. S4*B*; $d' = 1.14$; $t_{17} = 2.48$; $P = 0.024$) along the direction of the right VOF compared with the poor stereoacuity group. These differences in MTV and FA between the two groups were consistent with the results of the regression analysis of the microstructural properties of the right VOF and stereoacuity (Fig. 2*B* for MTV and *SI Appendix*, Fig. S4*A* for FA). We also found a significant group difference in axial diffusivity ($d' = 1.07$, $t_{17} = 2.33$, $P = 0.032$) but not radial diffusivity of the right VOF (*SI Appendix*, Fig. S5 *C* and *D*). The spatial profile of the tract properties suggested that the group difference was present along the entire length of the right VOF, from dorsal to ventral (Fig. 2*C* for MTV and *SI Appendix*, Fig. S4*B* for FA), and not restricted to a localized region. Thus, it is unlikely that the group difference can be explained by a partial volume effect with other short-range fibers (such as U-fibers). We did not find any significant differences in MTV and FA between the two groups in any other

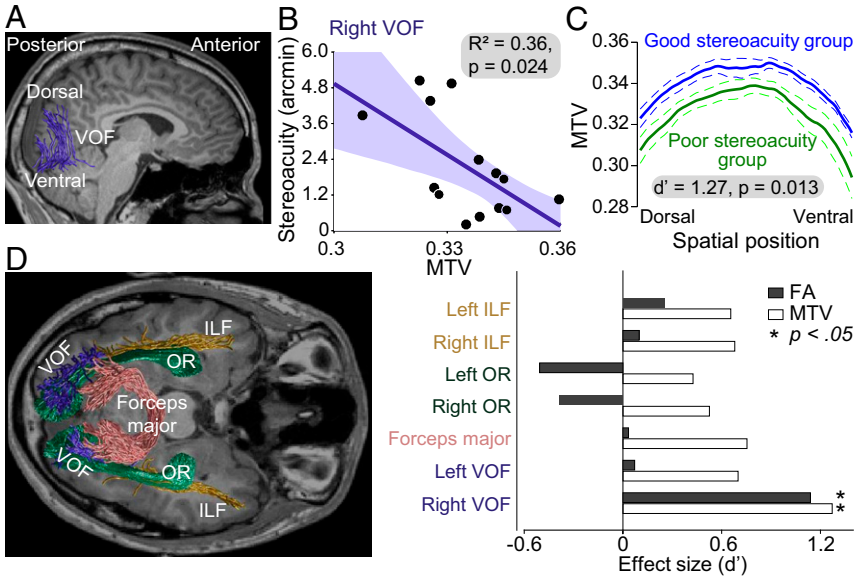


**Fig. 2.** Tissue property of the right VOF explains variabilities in human stereoacuity. (*A*) VOF in the right hemisphere identified in one representative participant (P9). VOF connects the dorsal and ventral regions of the occipital cortex. (*B*) Correlation between MTV of the right VOF and stereoacuity [$n$ = 14; $R^2$ = 0.36, $F_{(1,12)}$ = 6.71, $P$ = 0.024]. The shaded area represents 95% confidence intervals derived from bootstrapping. See *SI Appendix*, Fig. S4*A* for the correlation between FA of the right VOF and stereoacuity. (*C*) Tissue properties along the right VOF in good and poor stereoacuity groups. The vertical and horizontal axes represent the MTV and spatial position along the right VOF, respectively. The good stereoacuity group (blue, $n$ = 10) showed significantly higher MTV than the poor stereoacuity group (green, $n$ = 9) along the entire portion of the right VOF [$d'$ = 1.27, $t_{17}$ = 2.77, $P$ = 0.013, two-sample $t$ test]. Data are represented as mean (solid line) ± SEM (dotted line). (*D*) *Left* depicts the visual white matter tracts estimated by tractography (green, OR; pink, forceps major; dark yellow, ILF; blue, VOF) in one representative participant (P9). *Right* shows the effect size ($d'$) of the FA and MTV differences in each visual white matter tract between the good and poor stereoacuity groups. Positive or negative values represent index values that are larger or smaller in the good or poor stereoacuity group, respectively. *$P$ < 0.05, two-sample $t$ test. The effect size was largest in the right VOF in the two independent measurements (FA and MTV). There were no significant stereoacuity-dependent differences in the FA or MTV of the other visual white matter tracts.

visual white matter tracts, such as the ILF or OR in both hemispheres, forceps major, and left VOF (Fig. 2*D*). Furthermore, it should be noted that the difference in stereoacuity between these two groups was not accompanied by differences in refractive power or pupillary distance of the eyes (*SI Appendix*, Fig. S1*B*) nor age ($d'$ = 0, $t_{17}$ = 0, $P$ = 1; 25 ± 5.2 and 25 ± 3.7 y old for good and poor stereoacuity groups, respectively).

We found significant associations between MTV/FA and stereoacuity in the right, but not the left, VOF. We evaluated the robustness of the lateralization across different statistical criteria for rejecting VOF streamlines (*SI Appendix*, Fig. S6*A*). Although the regression analysis did not reach significance (*SI Appendix*, Fig. S6*B*), MTV along the left VOF showed marginally significant group difference in relatively conservative outlier rejection criteria ($d'$ = 0.91, $t_{17}$ = 1.99, $P$ = 0.063; *SI Appendix*, Fig. S6*C*). We noted that a significant effect in the right VOF was preserved in the conservative criterion ($d'$ = 1.20, $t_{17}$ = 2.62, $P$ = 0.018). These results suggest that a lack of statistical significance in the left VOF may be at least partly explained by the relative difficulty in identifying coherent streamlines.

In the above analysis, we estimated stereoacuity by pooling data from the left and right visual fields, which helped to improve the reliability of the estimate by increasing the number of trials. Given that the areas connected by VOF have retinotopic representation (26), we also tested the relationship between stereoacuity in left and right visual fields and the MTV of the contralateral VOF. The correlation between the right VOF and left stereoacuity was found to be marginally significant [$R^2$ = 0.27, $F_{(1,12)}$ = 4.39, $P$ = 0.058, *SI Appendix*, Fig. S2*C*], whereas the correlation between the left VOF and right stereoacuity was not significant [$R^2$ = 0.058, $F_{(1,12)}$ = 0.74, $P$ = 0.41, *SI Appendix*, Fig. S2*B*]. Group difference analysis also showed the same tendency (*SI Appendix*, Fig. S2 *D* and *E*). The lack of effect in the left VOF can be explained by multiple possible factors, such as a reduced reliability of stereoacuity estimates or difficulty in identifying coherent streamlines, as mentioned above.

**VOF Connects Cortical Regions Responding to Visual Stimuli with Binocular Disparity.** To test our hypothesis that the right VOF connects cortical areas that are involved in binocular disparity processing, we performed fMRI experiments to measure the cortical areas activated by the same RDSs as used in the psychophysical experiment (*Materials and Methods*). We observed significant BOLD responses to the RDSs, compared with uncorrelated RDSs, in both dorsal (V3A/B, IPS0) and ventral (hV4, VO1/2) extrastriate cortices that were consistent with previous fMRI studies in humans (Fig. 3*B*) (16, 30–32). Importantly, both dorsal and ventral VOF endpoints overlapped with disparity-selective regions (Fig. 3 and *SI Appendix*, *SI Materials and Methods*). These results agree with our hypothesis that discrimination of stereoscopic depth involves an interaction between dorsal and ventral cortices through the VOF. We note that we did not find any significant interhemispheric differences in BOLD responses to RDSs compared with uncorrelated RDSs (uRDSs) in the majority of retinotopic areas (V3, V3A/B, hV4, VO, LO) except for IPS0, which showed a stronger BOLD response in the right hemisphere ($d'$ = 0.60, $t_5$ = 2.58, $P$ = 0.0495, paired $t$ test, *SI Appendix*, Fig. S7).

**Psychophysical Experiment on Contrast Detection Sensitivity.** Finally, we addressed whether the tissue properties of the right VOF are also related to another visual performance that does not require binocular integration. We measured the thresholds of participants' contrast detection using Gabor patch stimuli (Fig. 4*A*). In contrast to disparity thresholds, contrast detection thresholds did not show a clear bimodal distribution (Fig. 4*B*), and were not significantly correlated with stereoacuity ($r$ = 0.08, $P$ = 0.82). A simple linear model that included the tissue properties of the right VOF did not significantly predict the contrast detection threshold [$R^2$ = 0.017, $F_{(1,17)}$ = 0.29, $P$ = 0.59 for FA; $R^2$ = 0.031, $F_{(1,17)}$ = 0.55, $P$ = 0.47 for MTV, Fig. 4*C*]. None of the other models using FA or MTV in the other white matter tracts significantly explained the variabilities of contrast detection threshold either (*SI Appendix*, Table S2). Group difference analysis revealed no significant difference in the tissue property of the right VOF between the good (low contrast threshold, $n$ = 12) and poor (high contrast threshold, $n$ = 7) contrast sensitivity groups (Fig. 4*D*; $d'$ = 0.21, $t_{17}$ = 0.44, $P$ = 0.66 for MTV; $d'$ = 0.16, $t_{17}$ = 0.34, $P$ = 0.74 for FA). Taken together, the variability of FA and MTV values did not correlate with the performance of the contrast detection that does not require binocular integration. Relation of the VOF to other visual tasks such as color or motion detection is an open question for future research.

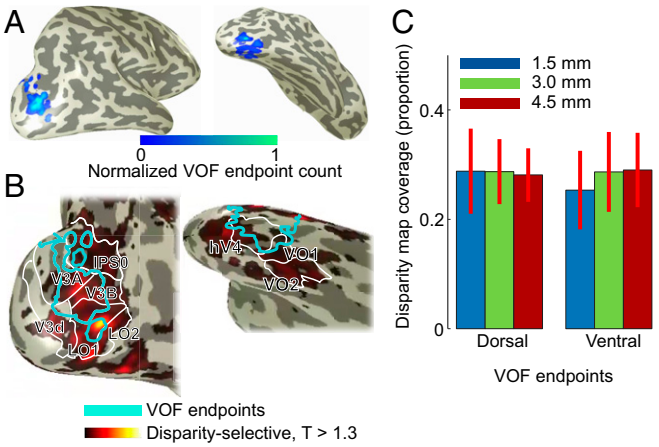


**Fig. 3.** Comparison between VOF endpoints and disparity-sensitive regions. (*A*) VOF endpoints in the right hemisphere from one representative participant, P8 (*Left*, dorsal view; *Right*, ventral view). Color maps on the cortical surface indicate a normalized count of VOF streamlines having endpoints within 3 mm from each gray matter voxel. (*B*) Disparity selective areas (hot color), which were significantly activated during the "RDS" blocks compared with the "uncorrelated RDS" blocks ($P < 0.05$, one-sample $t$ test). The borders of estimated VOF endpoints (cyan, identical in *A*) as well as the borders of visual areas (white) are overlaid. (*C*) Overlap between VOF endpoints and disparity selective regions in the right hemisphere. The vertical axis indicates the proportion of the gray matter voxels near VOF endpoints, which intersected with binocular disparity selective areas. The left and right three bars represent dorsal and ventral VOF endpoints, respectively. Different colored bars show data from varying distance thresholds for selecting the gray matter voxels near VOF endpoints (1.5 mm, blue; 3.0 mm, green; 4.5 mm, red). Disparity-selective regions overlap with similar proportion of VOF endpoints across the dorsal and ventral visual cortex. Data represent mean ± SEM ($n = 6$).

## Discussion

In the current study, we examined the neurobiological correlates of the large variability in stereoacuity. Advanced noninvasive neuroimaging methods, such as dMRI and qMRI, are advantageous when investigating the neurobiological origin of individual variance in sensory abilities because neuroanatomical and behavioral measurements collected from the same participants can be compared (33). We have used this advantage to compare human stereoacuity and white matter properties. We found a significant statistical relationship between stereoacuity and the microstructural properties in the right VOF, a specific white matter tract that connects the dorsal and ventral visual cortices (25, 26). These data support classical and recent theories that emphasize the importance of white matter tracts in understanding sensory and cognitive functions (34, 35). The behavior-anatomy correlates were found using the MTV and FA, two independent microstructural measurements, in both regression and group comparison analyses. Furthermore, we confirmed that the VOF had endpoints in disparity responsive regions of the dorsal and ventral cortices, suggesting that the VOF connects cortical regions that are involved in disparity processing. Finally, we found that the tissue properties of the right VOF were not related to contrast sensitivity.

A number of previous studies have used conventional diffusion tensor metrics, such as FA, to examine the tissue properties of white matter tracts relative to behavioral characteristics (33). In contrast, few recent studies have used advanced qMRI metrics, such as MTV (29), to assess the microstructural properties of white matter tracts. FA is a reproducible metric with high sensitivity for detecting the tissue structural differences in white matter tracts (33, 36). However, the microstructural interpretation of differences in FA is challenging because FA measurements can be associated with many biological factors, such as axon diameter, axon density, myelin-sheath thickness, and tightness of fasciculation due to crossing fibers (28, 36). Here, we combined dMRI with qMRI, which can provide additional information for inferring microstructural properties (29, 37). The MTV is a robust qMRI-based metric that quantifies local tissue volume within each voxel via quantification of proton density (29). There is converging evidence indicating that MTV is a reliable approximation of lipid and macromolecular volume fractions (38). While MTV has been used to quantify white matter tissue properties, this study demonstrates the relevance of MTV with behavioral measurements. Taken together, the relationship between the right VOF and stereoacuity, as shown in both FA and MTV analyses, may reflect a difference in lipid or macromolecule volume fractions, such as myelin thickness or axon density, rather than the morphological configuration of axons, such as the degree of fiber crossings.

Duan et al. (39) have investigated the microstructural properties of visual white matter tracts between amblyopia and control groups. They observed a difference in the diffusion property (mean diffusivity) along the right VOF; however, this difference is not supported by qMRI measurements. Additionally, Duan et al. reported a difference in the diffusion property along the optic radiation, which we did not find in this study. Our results and those of Duan et al. (39) suggest that the microstructural basis of stereoacuity is distinct from that of amblyopia.

Some visual neuroscience studies have emphasized the role of the dorsal stream in stereopsis (40–42), which is consistent with

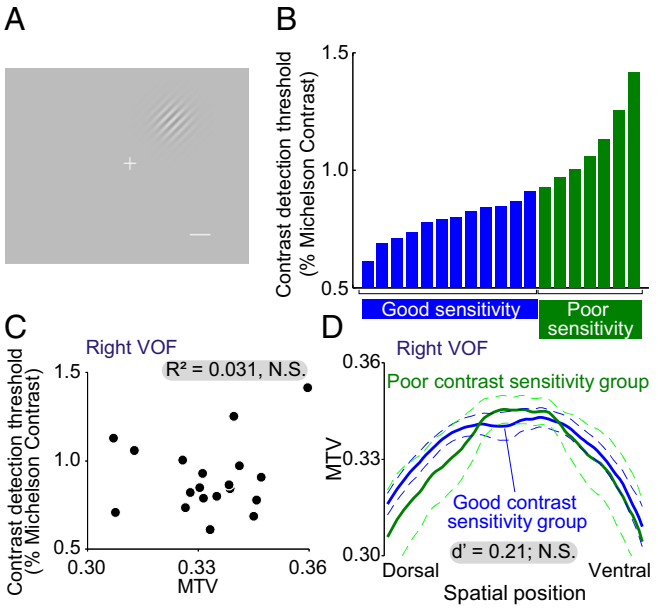


**Fig. 4.** The tissue properties of the right VOF do not explain variabilities in contrast sensitivity. (*A*) Gabor patch stimuli were used to measure contrast sensitivity. The white scale bar depicts 1°, which was not visible in the experiment. (*B*) The contrast sensitivity of all participants ($n = 19$; four of them were new participants who had not participated in the stereoacuity experiment). We classified participants into good (blue) and poor contrast sensitivity groups (green), respectively. This grouping is totally independent of the grouping in the stereoacuity experiment (Fig. 1*C*). (*C*) Scatter plot of MTV along the right VOF (horizontal axis) and contrast detection threshold of each participant. The MTV along the right VOF did not significantly predict the contrast detection threshold [$R^2 = 0.031$, $F_{(1,17)} = 0.55$, $P = 0.47$]. (*D*) MTV along right VOF in the good and poor contrast sensitivity groups. We did not find a significant difference in MTV between the groups ($d' = 0.21$, $t_{17} = 0.44$, $P = 0.66$). Data represent mean ± SEM. The conventions are identical to those in Fig. 2*C*.

experimental evidence showing the neural correlates of stereoscopic depth perception in dorsal areas (43); however, there are converging lines of evidence showing that not only dorsal but also ventral visual cortices are involved in binocular disparity processing, including computations of relative disparity and disparity-defined 3D shapes (11, 13, 14, 16, 30, 44–51). Other studies have suggested that the role of dorsal and ventral streams in stereopsis may be complementary because they are sensitive to different types of disparity information (7, 16–19, 52). Moreover, cortical representations that account for some aspects of binocular depth perception are found in higher regions of both the dorsal and ventral visual streams (31, 53), including cortical areas near the VOF endpoints (26). Here, we found that stereoacuity is correlated with the properties of the VOF (Fig. 2). In addition, we have confirmed that the endpoints of the VOF overlap with disparity selective regions (Fig. 3 *B* and *C*). Therefore, the VOF may transmit perceptually relevant signals of disparity by connecting the dorsal and ventral cortices involved in binocular disparity processing.

We consider that the behavioral–structural relationship in the VOF may be explained by either or both of two potential factors: strategies of stereo perception that altered white matter or white matter plasticity altered stereo perception. Recent neurobiological studies have demonstrated that plasticity in the white matter microstructure, such as the degree of myelination, is dependent on neural activity or behavioral experience (54, 55). We speculate that the behavioral–structural relationship observed in this study might reflect differences in development, such as different levels of usage of binocular disparity as a stereo cue, or cue combination strategies across dorsal and ventral visual areas. Alternatively, it is also feasible that development of white matter, which has a significant impact on the efficient conduction of neural signals, will affect the accuracy of stereo perception. However, it is not yet understood how such modulation in conduction velocity is related to the optimality of neural computation for sensory discrimination (55).

While we have shown a significant relationship between the right VOF and stereoacuity, we did not find statistically significant results for the left VOF. This asymmetry may result from a difference in technical detectability of the VOFs in the two hemispheres using tractography, probably because of a difference in the geometry of the sulcus and gyrus patterns. An additional analysis with multiple streamline exclusion criteria supports this interpretation (*SI Appendix*, Fig. S6). Alternatively, this asymmetry of the VOF may reflect a functional lateralization of cortical processing of binocular disparity, as reported in previous neuropsychological or fMRI studies (4, 15, 30, 32, 56, 57). However, this interpretation of right hemispheric dominance in stereopsis is puzzling when one considers the fact that V3A/B and hV4 in both hemispheres primarily cover the contralateral visual field and there was no or little difference in disparity discrimination performance (*SI Appendix*, Fig. S2*A*) and BOLD responses (*SI Appendix*, Fig. S7) between the left and right visual fields.

dMRI studies have focused on relatively long-range white matter tracts known to exist from anatomical studies (35). However, one might argue that fibers from other areas, such as V2 or MT, may also explain the variability on human stereoacuity. We cannot exclude this possibility. Measuring such relatively short fibers requires a substantial improvement in data resolution, analysis methods, and anatomical knowledge of the human visual system. Furthermore, the resolution of our dMRI data did not allow us to reliably identify subcomponents of VOF terminating in/near specific areas. Testing those questions with improved measurement techniques is an important future research direction.

In summary, the microstructural properties of the VOF explain the variability in human stereoacuity. Stereoacuity may be related to the microstructural properties of white matter pathway that supports communication between the dorsal and ventral visual cortices.

## Materials and Methods

The code for reproducing psychophysical experiments and analyses is publicly available in OSF.io (https://osf.io/qd8cj/). The full anonymized dataset, which are collected from participants who provided a written informed consent on the data sharing (22 of 23 participants as of September 4, 2018), will be available upon request to the corresponding author (htakemur@nict.go.jp).

**Participants.** Twenty-three healthy volunteers (19 males, 4 females; mean age, 26.1 y old) participated in the study. None of the participants had a history of eye disease. All participants gave written informed consent to take part in this study, which was conducted in accordance with the ethical standards stated in the Declaration of Helsinki and approved by the local ethics and safety committees at the Center for Information and Neural Networks (CiNet), National Institute of Information and Communications Technology.

**Stereoacuity Experiment.** Nineteen participants (16 males, 3 females; mean age, 25.0 y old) took part in the experiment to determine their stereoacuity. The stereoacuity experiment employed a haploscope. Each eye viewed one-half of the monitor through an angled mirror and a front triangular prism mirror. Each RDS was composed of a central disk (diameter: 3°) and surrounding ring (width: 0.5°, outer diameter: 4°; see *SI Appendix*, Fig. S1*A* for an example). The surrounding ring always had zero disparity, whereas the binocular disparity in the central disk varied across trials (disparity magnitudes: ±0.12–7.68 arcmin), which were chosen based on a typical range of human stereoacuity (22). In each trial, an RDS was presented at one of four different positions (Up-Right, Up-Left, Down-Right, and Down-Left), whose center was 3° away from the fixation point. Participants judged whether the central disk appeared nearer or farther than the surrounding ring while fixating on the central fixation point (*SI Appendix*, Fig. S1*A*). We defined stereoacuity as the magnitude of binocular disparity that corresponded to the 84% correct rate in the task by fitting a cumulative Gaussian psychometric function. See *SI Appendix, SI Materials and Methods* for further technical details.

**Contrast Threshold Experiment.** Nineteen participants (15 males, 4 females; mean age, 26.0 y old) underwent a contrast threshold experiment. Fifteen of these participants also participated in the stereoacuity experiment. We presented Gabor patch stimuli whose orientation was tilted 45° to the left or right from vertical (Fig. 4*A*). Participants were asked to judge whether the stimulus orientation was tilted toward the left or right. The stimulus positions were identical to those used in the stereoacuity experiment. The experiment composed of two stages. An approximate threshold was measured in the first stage, which was used to determine the contrast range that was used at the second stage to estimate a precise threshold. See *SI Appendix, SI Materials and Methods* for further technical details.

**Structural MRI Experiment.** All MRI data were acquired using a 3T SIEMENS Trio Tim scanner at CiNet, National Institute of Information and Communications Technology, and Osaka University.

We collected dMRI data (2 mm isotropic) from all participants ($n$ = 23) using a 32-channel head coil. The diffusion weighting was isotropically distributed along the 64 directions ($b$ = 1,000 s/mm$^2$). Nondiffusion-weighted ($b$ = 0) images were acquired at the beginning and end of the dMRI session (two $b$ = 0 acquisitions per image set). Acquisition of the dMRI data took ∼20 min for each participant.

We collected qMRI data from all participants ($n$ = 23) using a 32-channel head coil. qMRI measurements (1 mm isotropic) were obtained using protocols described in a previous publication (29). Acquisition of the qMRI data took ∼35 min for each participant.

Further details in structural MRI data acquisition and preprocessing methods are described in *SI Appendix, SI Materials and Methods*.

**Diffusion MRI Data Analysis.** dMRI data preprocessing was performed using mrDiffusion tools implemented in the vistasoft distribution (https://github.com/vistalab/vistasoft). We identified visual white matter tracts in each participant, from whole-brain streamline generated by probabilistic tractography implemented in MRtrix3 (www.mrtrix.org/) (58) and selected by Linear Fascicle Evaluation (LiFE; https://francopestilli.github.io/life/) (59). Details are described in *SI Appendix, SI Materials and Methods*.

**Quantitative MRI Data Analysis.** qMRI data were processed using the mrQ software package (https://github.com/mezera/mrQ) to produce the MTV maps (29). Details are described in *SI Appendix, SI Materials and Methods*.

**Functional MRI Experiment.** We collected fMRI data from eight participants who participated in the stereoacuity psychophysical experiment (seven males, one female; mean age, 26.6 y old). We used the posterior section of a 32-channel coil. Data were acquired at a resolution of 2.0-mm isotropic voxels with an interleaved T2*- weighted gradient echo sequence. Participants viewed gray background, RDS, or uRDS through a polarized 3D system, during which they performed a fixation task requiring vernier detection (31). We excluded two participants with poor task performance during the fMRI scan (<84% correct rate) from subsequent analyses. The disparity-selective areas are defined as cortical gray matter voxels that responded more strongly to RDS than uRDS ($P < 0.05$, one-sample $t$ test). Acquisition of fMRI data took ∼60 min for each participant. See *SI Appendix, SI Materials and Methods* for further technical details.

**Tract Identifications and Evaluations.** We identified seven white matter tracts (left and right ILF, left and right OR, forceps major, and left and right VOF) from dMRI dataset. We then evaluated the tissue properties of each tract and summarized the profile of each tract with a vector of 80 values representing the FA or MTV values sampled at equidistant locations along the central portion of the tract. The relationship between tract properties and psychophysical performance was evaluated in regression and group comparison analyses. Further details are described in *SI Appendix, SI Materials and Methods*.

**ACKNOWLEDGMENTS.** We thank Atsushi Wada for providing the computing environment; Aviv Mezer, Garikoitz Lerma-Usabiaga, and Takashi Ueguchi for the suggestion on qMRI data collection; Thomas Baumgartner for his participation in an initial stage of this study; and Hiroshi Ban, Nobuhiro Hagura, Franco Pestilli, and Brian A. Wandell for comments on an earlier version of the manuscript. This study was supported by Japan Society for the Promotion of Science (JSPS) KAKENHI (Grants JP15J00412 and JP17H04684 to H.T., JP16H01673 and JP18H05007 to I.F., JP16H05862 to K.A.) and "Program for Leading Graduate Schools" Grant of the Ministry of Education, Culture, Science and Technology, Japan (to H.O.). This study was also supported by a grant from the Ministry of Internal Affairs and Communications (to I.F.).

1. Wheatstone C (1838) Contributions to the physiology of vision.–Part the first. On some remarkable, and hitherto unobserved, phenomena of binocular vision. *Philos Trans R Soc Lond B Biol Sci* 128:371–394.
2. Julesz B (1971) *Foundations of Cyclopean Perception* (Univ Chicago Press, Chicago).
3. Marr D, Poggio T (1976) Cooperative computation of stereo disparity. *Science* 194: 283–287.
4. Howard IP, Rogers BJ (1995) *Binocular Vision and Stereopsis* (Oxford Univ Press, New York).
5. Ponce CR, Born RT (2008) Stereopsis. *Curr Biol* 18:R845–R850.
6. Blake R, Wilson H (2011) Binocular vision. *Vision Res* 51:754–770.
7. Fujita I, Doi T (2016) Weighted parallel contributions of binocular correlation and match signals to conscious perception of depth. *Philos Trans R Soc Lond B Biol Sci* 371: 20150257.
8. Ohzawa I, DeAngelis GC, Freeman RD (1990) Stereoscopic depth discrimination in the visual cortex: Neurons ideally suited as disparity detectors. *Science* 249:1037–1041.
9. Parker AJ (2007) Binocular depth perception and the cerebral cortex. *Nat Rev Neurosci* 8:379–391.
10. Welchman AE (2016) The human brain in depth: How we see in 3D. *Annu Rev Vis Sci* 2: 345–376.
11. Janssen P, Vogels R, Orban GA (1999) Macaque inferior temporal neurons are selective for disparity-defined three-dimensional shapes. *Proc Natl Acad Sci USA* 96:8217–8222.
12. DeAngelis GC, Newsome WT (1999) Organization of disparity-selective neurons in macaque area MT. *J Neurosci* 19:1398–1415.
13. Uka T, Tanaka H, Yoshiyama K, Kato M, Fujita I (2000) Disparity selectivity of neurons in monkey inferior temporal cortex. *J Neurophysiol* 84:120–132.
14. Orban GA, Janssen P, Vogels R (2006) Extracting 3D structure from disparity. *Trends Neurosci* 29:466–473.
15. Bridge H (2016) Effects of cortical damage on binocular depth perception. *Philos Trans R Soc Lond B Biol Sci* 371:20150254.
16. Neri P, Bridge H, Heeger DJ (2004) Stereoscopic processing of absolute and relative disparity in human visual cortex. *J Neurophysiol* 92:1880–1891.
17. Uka T, DeAngelis GC (2006) Linking neural representation to function in stereoscopic depth perception: Roles of the middle temporal area in coarse versus fine disparity discrimination. *J Neurosci* 26:6791–6802.
18. Shiozaki HM, Tanabe S, Doi T, Fujita I (2012) Neural activity in cortical area V4 underlies fine disparity discrimination. *J Neurosci* 32:3830–3841.
19. Chang DHF, Mevorach C, Kourtzi Z, Welchman AE (2014) Training transfers the limits on perception from parietal to ventral cortex. *Curr Biol* 24:2445–2450.
20. Richards W (1970) Stereopsis and stereoblindness. *Exp Brain Res* 10:380–388.
21. Movshon JA, Chambers BE, Blakemore C (1972) Interocular transfer in normal humans, and those who lack stereopsis. *Perception* 1:483–490.
22. Zaroff CM, Knutelska M, Frumkes TE (2003) Variation in stereoacuity: Normative description, fixation disparity, and the roles of aging and gender. *Invest Ophthalmol Vis Sci* 44:891–900.
23. Hess RF, To L, Zhou J, Wang G, Cooperstock JR (2015) Stereo vision: The haves and have-nots. *Iperception* 6:2041669515593028.
24. Yeatman JD, Rauschecker AM, Wandell BA (2013) Anatomy of the visual word form area: Adjacent cortical circuits and long-range white matter connections. *Brain Lang* 125:146–155.
25. Yeatman JD, et al. (2014) The vertical occipital fasciculus: A century of controversy resolved by in vivo measurements. *Proc Natl Acad Sci USA* 111:E5214–E5223.
26. Takemura H, et al. (2016) A major human white matter pathway between dorsal and ventral visual cortex. *Cereb Cortex* 26:2205–2214.
27. Wichmann FA, Hill NJ (2001) The psychometric function: I. Fitting, sampling, and goodness of fit. *Percept Psychophys* 63:1293–1313.
28. Basser PJ, Pierpaoli C (1996) Microstructural and physiological features of tissues elucidated by quantitative-diffusion-tensor MRI. *J Magn Reson B* 111:209–219.
29. Mezer A, et al. (2013) Quantifying the local tissue volume and composition in individual brains with magnetic resonance imaging. *Nat Med* 19:1667–1672.
30. Tsao DY, et al. (2003) Stereopsis activates V3A and caudal intraparietal areas in macaques and humans. *Neuron* 39:555–568.
31. Preston TJ, Li S, Kourtzi Z, Welchman AE (2008) Multivoxel pattern selectivity for perceptually relevant binocular disparities in the human brain. *J Neurosci* 28: 11315–11327.
32. Ip IB, Minini L, Dow J, Parker AJ, Bridge H (2014) Responses to interocular disparity correlation in the human cerebral cortex. *Ophthalmic Physiol Opt* 34:186–198.
33. Wandell BA, Yeatman JD (2013) Biological development of reading circuits. *Curr Opin Neurobiol* 23:261–268.
34. Catani M, ffytche DH (2005) The rises and falls of disconnection syndromes. *Brain* 128: 2224–2239.
35. Catani M, Thiebaut de Schotten M (2012) *Atlas of Human Brain Connections* (Oxford Univ Press, Oxford).
36. Assaf Y, Johansen-Berg H, Thiebaut de Schotten M (July 11, 2017) The role of diffusion MRI in neuroscience. *NMR Biomed*, 10.1002/nbm.3762.
37. Weiskopf N, Mohammadi S, Lutti A, Callaghan MF (2015) Advances in MRI-based computational neuroanatomy: From morphometry to in-vivo histology. *Curr Opin Neurol* 28:313–322.
38. Duval T, et al. (2017) g-Ratio weighted imaging of the human spinal cord *in vivo*. *Neuroimage* 145:11–23.
39. Duan Y, Norcia AM, Yeatman JD, Mezer A (2015) The structural properties of major white matter tracts in strabismic amblyopia. *Invest Ophthalmol Vis Sci* 56:5152–5160.
40. Hubel DH, Livingstone MS (1987) Segregation of form, color, and stereopsis in primate area 18. *J Neurosci* 7:3378–3415.
41. Sakata H, Taira M, Kusunoki M, Murata A, Tanaka Y (1997) The TINS lecture. The parietal association cortex in depth perception and visual control of hand action. *Trends Neurosci* 20:350–357.
42. Gonzalez F, Perez R (1998) Neural mechanisms underlying stereoscopic vision. *Prog Neurobiol* 55:191–224.
43. Minini L, Parker AJ, Bridge H (2010) Neural modulation by binocular disparity greatest in human dorsal visual stream. *J Neurophysiol* 104:169–178.
44. Cowey A, Porter J (1979) Brain damage and global stereopsis. *Proc R Soc Lond B Biol Sci* 204:399–407.
45. Ptito A, Zatorre RJ, Larson WL, Tosoni C (1991) Stereopsis after unilateral anterior temporal lobectomy. Dissociation between local and global measures. *Brain* 114: 1323–1333.
46. Tanaka H, Uka T, Yoshiyama K, Kato M, Fujita I (2001) Processing of shape defined by disparity in monkey inferior temporal cortex. *J Neurophysiol* 85:735–744.
47. Gilaie-Dotan S, Ullman S, Kushnir T, Malach R (2002) Shape-selective stereo processing in human object-related visual areas. *Hum Brain Mapp* 15:67–79.
48. Chandrasekaran C, Canon V, Dahmen JC, Kourtzi Z, Welchman AE (2007) Neural correlates of disparity-defined shape discrimination in the human brain. *J Neurophysiol* 97: 1553–1565.
49. Cottereau BR, McKee SP, Ales JM, Norcia AM (2011) Disparity-tuned population responses from human visual cortex. *J Neurosci* 31:954–965.
50. Bridge H, et al. (2013) Structural and functional changes across the visual cortex of a patient with visual form agnosia. *J Neurosci* 33:12779–12791.
51. Umeda K, Tanabe S, Fujita I (2007) Representation of stereoscopic depth based on relative disparity in macaque area V4. *J Neurophysiol* 98:241–252.
52. Doi T, Tanabe S, Fujita I (2011) Matching and correlation computations in stereoscopic depth perception. *J Vis* 11:1.
53. Bridge H, Parker AJ (2007) Topographical representation of binocular depth in the human visual cortex using fMRI. *J Vis* 7:1–14.
54. Sampaio-Baptista C, et al. (2013) Motor skill learning induces changes in white matter microstructure and myelination. *J Neurosci* 33:19499–19503.
55. Fields RD (2015) A new mechanism of nervous system plasticity: Activity-dependent myelination. *Nat Rev Neurosci* 16:756–767.
56. Murphy AP, Leopold DA, Humphreys GW, Welchman AE (2016) Lesions to right posterior parietal cortex impair visual depth perception from disparity but not motion cues. *Philos Trans R Soc Lond B Biol Sci* 371:20150267.
57. Gillebert CR, et al. (2015) 3D shape perception in posterior cortical atrophy: A visual neuroscience perspective. *J Neurosci* 35:12673–12692.
58. Tournier JD, Calamante F, Connelly A (2012) MRtrix: Diffusion tractography in crossing fiber regions. *Int J Imaging Syst Technol* 22:53–66.
59. Pestilli F, Yeatman JD, Rokem A, Kay KN, Wandell BA (2014) Evaluation and statistical inference for human connectomes. *Nat Methods* 11:1058–1063.